Colloids and Surfaces B: Biointerfaces 196 (2020) 111343

Contents lists available at ScienceDirect

Colloids and Surfaces B: Biointerfaces

journal homepage: www.elsevier.com/locate/colsurfb

A facile surface modification of poly(dimethylsiloxane) with amino acid conjugated self-assembled monolayers for enhanced osteoblast cell behavior

M. Özgen Öztürk-Öncel [a], Sedat Odabaş [b], Lokman Uzun [c], Deniz Hür [d], Bora Garipcan [a,*]

[a] Boğaziçi University, Institute of Biomedical Engineering, Istanbul, Turkey
[b] Ankara University, Department of Chemistry, Ankara, Turkey
[c] Hacettepe University, Department of Chemistry, Ankara, Turkey
[d] Eskisehir Technical University, Department of Chemistry, Eskisehir, Turkey

ARTICLE INFO

Keywords:
Polydimethylsiloxane
Self-assembled monolayers
Surface modification
Amino acid
Human fetal osteoblast

ABSTRACT

Polydimethylsiloxane (PDMS) is a biocompatible synthetic polymer and used in various applications due to its low toxicity and tunable surface properties. However, PDMS does not have any chemical cues for cell binding. Plasma treatment, protein coating or surface modification with various molecules have been used to improve its surface characteristics. Still, these techniques are either last for a very limited time or have very complicated experimental procedures. In the present study, simple and one-step surface modification of PDMS is successfully accomplished by the preparation of hydrophilic and hydrophobic amino acid conjugated self-assembled monolayers (SAMs) for enhanced interactions at the cell-substrate interface. Synthesis of histidine and leucine conjugated (3-aminopropyl)-triethoxysilane (His-APTES and Leu-APTES) were confirmed with proton nuclear magnetic resonance spectroscopy (^{1}H NMR) and optimum conditions for the modification of PDMS with SAMs were investigated by X-ray photoelectron spectroscopy (XPS) analysis, combined with water contact angle (WCA) measurements. Results indicated that both SAMs enhanced cellular behavior *in vitro*. Furthermore, hydrophilic His-APTES modification provides a superior environment for the osteoblast maturation with higher alkaline phosphatase activity and mineralization. As histidine, leucine, and functional groups of these SAMs are naturally found in biological systems, modification of PDMS with them increases its cell-substrate surface biomimetic properties. This study establishes a successful modification of PDMS for *in vitro* cell studies, offering a biomimetic and easy procedure for potential applications in microfluidics, cell-based therapies, or drug investigations.

1. Introduction

PDMS has been attracted much attention in the biomedical area for developing cell culture substrates [1,2], medical implants [3,4], organs-on-chips [5,6], and microfluidic devices [7,8]. Comparable biocompatibility, low-toxicity, high oxygen permeability, low cost, ease of fabrication, and desirable elastic properties are some of the superior characteristics of PDMS, provoking its extensive use as a biomaterial. However, in its native form, PDMS possesses a highly hydrophobic surface that leads to poor cell adhesion and proliferation [9]. Thus, there is a high demand for PDMS with enhanced surface properties and increased stability to provide a convenient environment for specific cell functions.

Numerous techniques have been developed to improve surface characteristics of PDMS. A conventional and straightforward approach is increasing the substrate wettability by exposing to oxygen plasma [10], UV/ozone [11], or corona discharge [12]. Even though each of these treatments provides hydrophilic surfaces, long term stability cannot be achieved due to the hydrophobic recovery of PDMS [13]. This phenomenon results in an increased delamination tendency of cells from PDMS surfaces only a few days after seeding [14]. Extracellular matrix (ECM) protein coatings have also been widely used to produce cell microenvironment-like surfaces, leading to improved biocompatibility and enhanced cell behavior [15]. However, these interactions of proteins with surfaces are regulated by weak forces. As a result, cells on these surfaces tend to detach or being aggregated after they reached confluence due to protein dissociation [16,17]. To achieve strong linkages, APTES has been used for incorporating functional amine groups on

* Corresponding author at: Boğaziçi University, Institute of Biomedical Engineering, Kandilli Kampus, Uskudar, 34684, Istanbul, Turkey.
E-mail address: bora.garipcan@boun.edu.tr (B. Garipcan).

https://doi.org/10.1016/j.colsurfb.2020.111343
Received 6 May 2020; Received in revised form 12 August 2020; Accepted 19 August 2020
Available online 27 August 2020

the PDMS surface. Then, ECM components have been introduced to these aminated surfaces, by using ionic interactions that are stronger than weak van der Waals forces. This approach is a relatively an easy approach and showed better cell adhesion and proliferation than protein adsorption on PDMS [18]. There is a growing interest in using APTES, a self-assembled monolayer (SAM), to obtain stabilized modification on PDMS. APTES modified PDMS surfaces have also been used for cell culture environments as an intermediate modification step during the addition of glutaraldehyde or 1-ethyl-3- (3-dimethylaminopropyl) carbodiimide (EDC)/N-hydroxysuccinimide (NHS) chemistries for protein immobilization procedures [17–19]. Although all these surface treatment techniques have applied efficient SAM stabilization with cell microenvironment components, their modification procedures are quite challenging and require many experimental steps.

Among many different surface modification methods for enhanced cell interaction purposes, SAMs provide superior advantages with their well-defined, stable and tunable surface chemistry on various types of substrates [20] and easy preparation without any need of expensive and high-level equipment [21,22]. SAMs modified surfaces have been reported for diverse applications, including drug delivery [23], biosensors [24], biomolecule immobilization [25], non-specific protein adsorption [26], in addition to their use in synthetic cell culture environments [27]. Keselowsky et al. showed the osteogenesis induction of MC3T3-E1 cells on −OH and -NH_2 functionalized surfaces [28]. Moreover, Curran et al. demonstrated that SAMs with different functional groups could also be used for stem cell differentiation. According to their report, methyl (−CH_3) modified surfaces provided mesenchymal stem cell (MSC) phenotype preservation, where amino (-NH_2) and silane (-SH) modified ones initiated osteogenic differentiation with or without any external stimuli [29]. Because these functional groups are found naturally in biological environments, the modification of cell substrates with SAMs plays a major role in regulating protein adsorption and cell behavior [21,30].

As SAMs are highly organized structures, they tune the wettability properties of surfaces depending on their functional groups [22]. Wettability is one of the most important characteristics of a cell substrate [31]. Hydrophilic surfaces were documented to enhance osteoblast growth *in vitro* [32,33]. Arima et al. showed the combined effects of surface wettability and functional groups of SAMs on adhesion of HeLa cells and human umbilical vein endothelial cells (HUVECs) [34].

In the present study, we reported cell and substratum interactions over the substrate surface wettability and functional groups through amino acid conjugated SAMs, by using human fetal osteoblastic cell line, hFOB 1.19 as a model. Essential amino acids are known to stimulate bone formation by enhancing alkaline phosphatase activity and collagen synthesis [35]. A recent work documented that hydrophilic hydroxyapatite/poly (amino acid) modified phosphodiester improved osteoblast adhesion, differentiation, and cranial bone formation [36]. Here, we prepared hydrophilic and hydrophobic amino acid conjugated SAMs and modified PDMS substrates with them to obtain stable, practical, and biomimetic substrate surfaces with varying wettability. By designing these amino acid incorporated SAMs, we aimed to enhance cell-biomaterial interactions and regulate biological signals, as extracellular matrix-like surfaces have the tendency of providing better cell culture environments. Here in this study, histidine and leucine conjugated SAM (His-APTES or Leu-APTES) modified PDMS substrates were optimized and characterized by using XPS and WCA analysis. The effects of these novel SAMs on osteoblast cell behavior were investigated for day 21 to see both osteogenic maturation of cells and long-term stability of modified PDMS substrates. Cell responses, such as proliferation, actin cytoskeleton formation, alkaline phosphatase activity, and extracellular matrix mineralization to native and SAMs modified PDMS, showed that the modification of PDMS with amino acid conjugated SAMs enhanced cell substrate properties of PDMS, specifically for osteoblastic behavior.

2. Material and methods

2.1. Preparation of PDMS substrates

PDMS substrates were prepared by mixing 10:1 (w/w) ratio of prepolymer and curing agent (Sylgard 184, Dow Corning), followed by degassing under vacuum for 30 min. PDMS mixture was then spin-coated onto glass coverslips (18 mm diameter) at 2000 rpm for 5 s (CEE 200X, Brewer Science) to obtain thin and flat substrates. Curing was performed at 60 °C for 24 h [37]. After the curing process, substrates were sonicated for 10 min in absolute ethanol and distilled water, respectively, and dried under N_2 stream.

2.2. Synthesis of His-APTES and Leu-APTES

His-APTES and Leu-APTES were synthesized following the previous method developed by the authors [38]. His-APTES and Leu-APTES synthesis procedure is based on the activation of carboxylic acid groups (−COOH) of carboxybenzyl (Cbz)-protected L-His−OH and L-Leu−OH using benzotriazole chemistry [39]. The intermediate products Cbz-L-Leu-Bt and Cbz-L-His-Bt were subsequently reacted with APTES in tetrahydrofuran (THF)in the presence of Et_3N as a base to synthesize Cbz-L-Leu-APTES and Cbz-L-His-APTES, respectively. These intermediates were deprotected under catalytic hydrogenation to give final products L-Leu-APTES and L-His-APTES (Fig. 1). ^1H NMR. (Bruker 500 MHz) was used for the characterization of His-APTES and Leu-APTES.

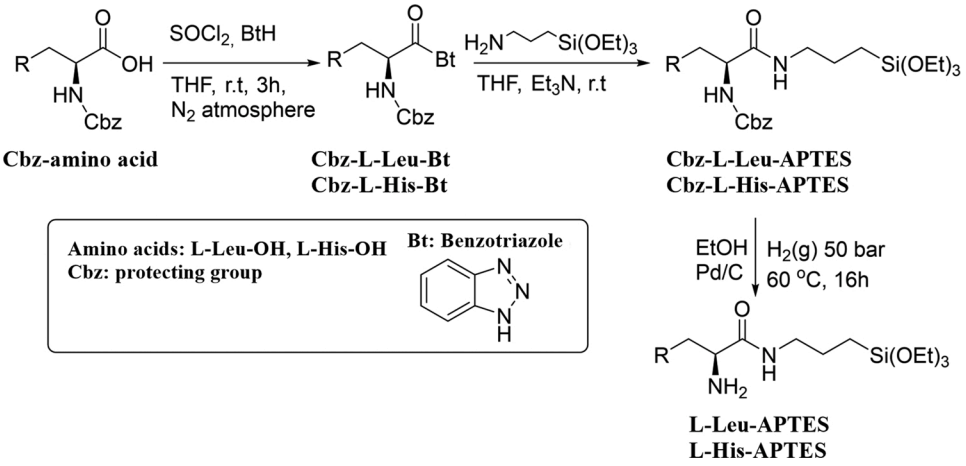

Fig. 1. The synthesis procedure of L-His-APTES and L-Leu-APTES.

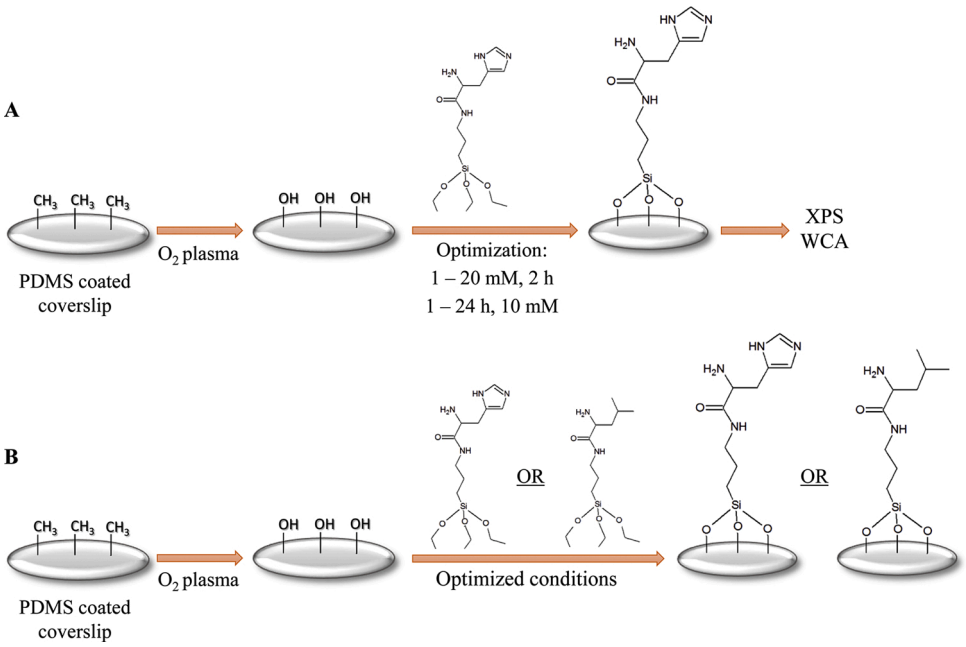

Fig. 2. Schematic illustration of PDMS modification. (A) Optimization of His-APTES modification (1-20 mM, 2 h and 10 mM, 1-24 h), and (B) modification of PDMS surface with His-APTES or Leu-APTES (10 mM, 24 h).

2.3. Modification of PDMS

Prior to modification with His-APTES and Leu-APTES, PDMS substrates were exposed to oxygen plasma for 1 min, at 200 mTorr and under 50 sccm oxygen flow (PM-100, March Plasma Systems) to produce reactive hydroxyl groups on surfaces without any alteration on the surface topography [40]. Surface modification conditions were optimized by using His-APTES as a model SAM. Activated PDMS substrates were immersed into His-APTES in ethanol, having different concentrations in the range of 1−20 mM at room temperature for two hours, followed by using a fixed concentration and varying dipping time in the range of 1–24 h. Leu-APTES modification was performed under optimized conditions. Following the functionalization, solutions were removed, and substrates were rinsed with absolute ethanol and distilled water three times. SAM modification procedure of PDMS was schematized in Fig. 2.

2.4. Surface characterization

Surfaces of PDMS substrates were characterized in terms of functionality and wettability with XPS and WCA, respectively. Modification of PDMS substrates with His-APTES and Leu-APTES was verified chemically by using and XPS with Al-Kα source gun (Thermo Scientific). Wide scans were recorded in the binding energy range of 1350−0 eV with 150 eV pass energy. Wettability of surfaces before and after modifications was investigated by using sessile drop water contact angle analysis (CAM-100, KSV Instruments). Measurements were carried out at room temperature by introducing 2 μL of distilled water droplets to the surfaces while recording the images for 10 s. For each experimental group, three random areas of five samples were measured.

Stability of SAMs modification was investigated with a model SAM: His-APTES, by the application of constant DI H_2O flow through the flow cell part of the Quartz Crystal Microbalance (QCM, QCM200, Stanford Research Systems). PDMS surfaces were characterized with XPS and WCA, before and after the flow application. The details are provided in the Supporting Information (SI).

2.5. Human osteoblastic cell culture

Human fetal osteoblast cells (hFOB 1.19, ATCC CRL-11,372) were used to investigate the effects of PDMS substrates with different surface chemistries. The cells were maintained and expanded in DMEM/F-12 (Sigma), supplemented with 10 % fetal bovine serum (FBS, Biosera) and 1 % antibiotic antimycotic solution (Biosera). The medium was changed every two days. When cells reached confluence, 0.25 % trypsin-EDTA solution (Sigma) was used to harvest them. Cells at passage number 5 were used. For the cell culture studies, PDMS substrates were rinsed with 70 % ethanol and sterile PBS, followed by exposure to UV light for 1 h. Then, the cells were cultured on the PDMS substrates in non-treated 12-well cell culture plates (SPL Life Sciences) with a seeding density of 50,000 cells/well. Cells were incubated in a humidified incubator at 37 °C with 5% CO_2 up to 21 days.

2.6. Cell proliferation assay

The proliferation of osteoblast cells on PDMS substrates was assessed by Alamar Blue assay for up to 7 days. At specific time points, culture media was replaced with the fresh one containing 10 % Alamar blue and incubated at 37 °C for 4 h. Then, optical absorbance values were measured at 570 and 595 nm by using a Micro-Plate Reader Spectrophotometer (BIO-RAD iMark) [41].

2.7. Actin cytoskeleton staining

The actin cytoskeleton of the cells on PDMS substrates, was explored using Alexa Fluor 488 Phalloidin (Thermo Fisher) staining at the end of day 7. Briefly, cells were rinsed twice with PBS and fixed in 4 % formaldehyde solution for 10 min, followed by rinsing with PBS three times for 5 min. To increase permeability, cells were immersed immediately in 0.1 % Triton X-100 in PBS for 5 min. Nonspecific bindings were blocked with 1 % BSA solution for 20 min. After the blocking step, Alexa Fluor 488 Phalloidin solution (in 1% BSA) was added to the cells. A counter-staining with DAPI was also performed to stain cell nuclei by incubating cells in DAPI staining solution (Thermo Fisher) for 3 min. Images were recorded under the fluorescence of excitation at 488 nm for f-actin cytoskeleton (green) and 358 nm for cell nuclei (blue) by using a

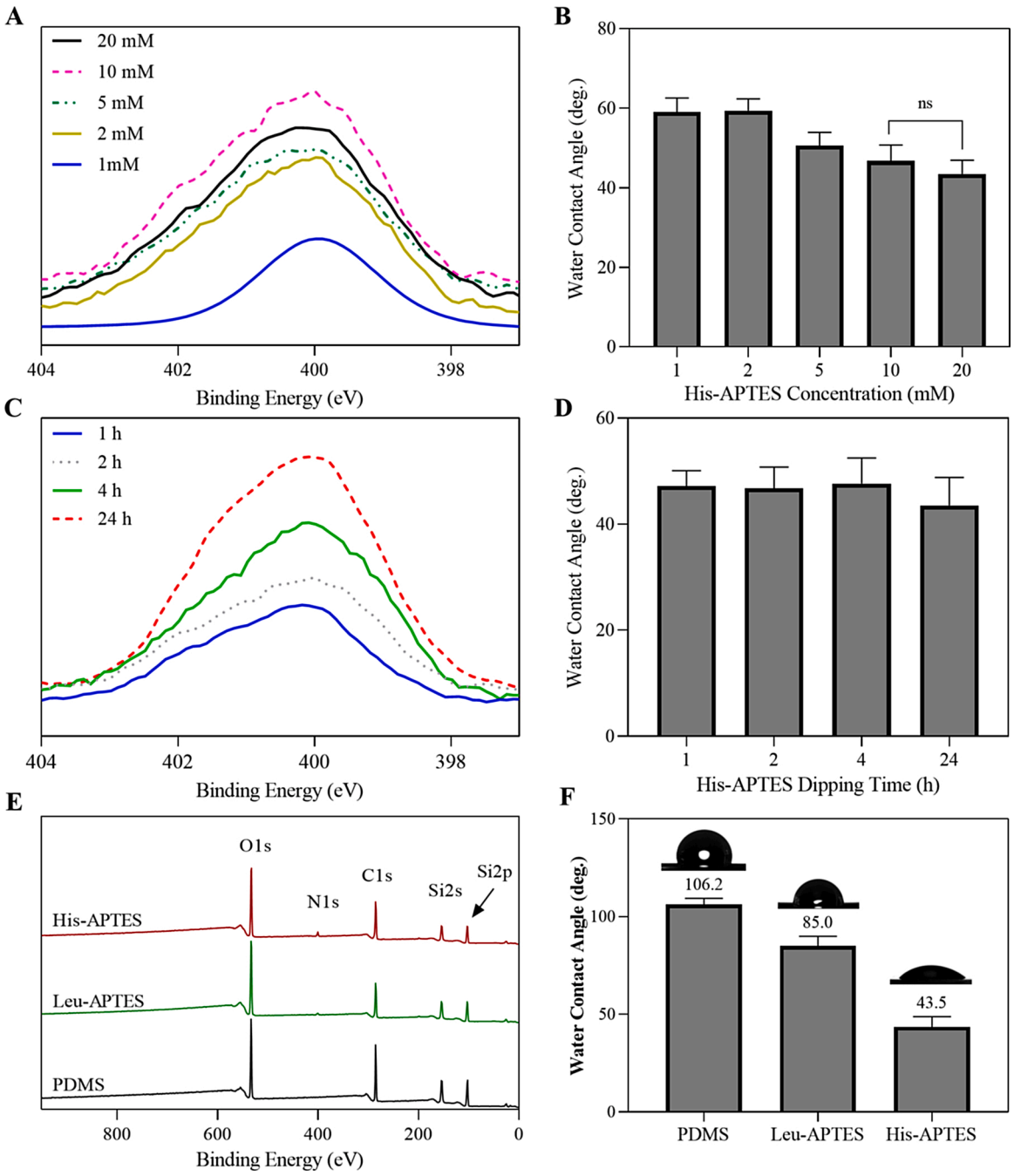

Fig. 3. (A) High-resolution N1s spectra and (B) WCA measurements of PDMS modified with increasing concentrations (1-20 mM) of His-APTES. (C) High-resolution N1s spectra and (D) WCA measurements for His-APTES modification of PDMS with increasing dipping time (1- 24 h). (E) XPS wide scan spectra of native, Leu-APTES modified, and His-APTES modified PDMS substrates. (F) WCAs of native, Leu-APTES modified, and His-APTES modified PDMS substrates.

Table 1
Surface elemental composition of native and SAMs modified PDMS substrates.

Substrates	Theoretical (%)				Measured (%)			
	Si	C	N	O	Si	C	N	O
PDMS	25	50	–	25	29.99	43.18	–	26.83
Leu-APTES	21.05	47.37	10.53	21.05	27.90	37.59	1.35	33.16
His-APTES	19	43	19	19	24.00	42.20	2.96	30.72

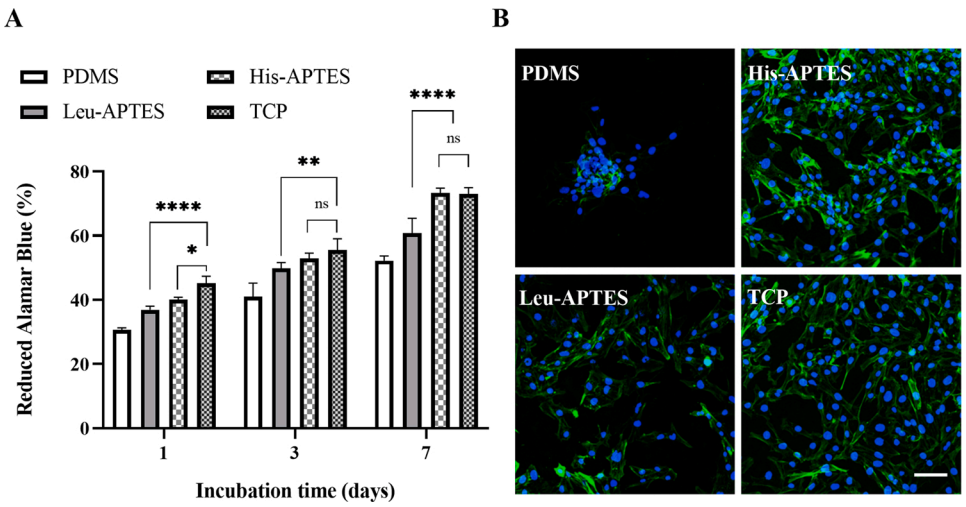

Fig. 4. (A) Reduced Alamar Blue percentages showing the relative hFOB cell proliferation on native, Leu-APTES, and His-APTES modified PDMS with positive control of TCP over 7 days. Data were given as means ± SD and $n = 7$. All groups were statistically significant respect to native PDMS, each day (****$p < 0.0001$; except for Leu-APTES on Day 1, ***$p < 0.001$), *$p < 0.05$, **$p = 0.01$. (B) Fluorescence images of Alexa Fluor 488-phalloidin (green) and DAPI (blue) stained hFOBs on native, Leu-APTES, and His-APTES modified PDMS substrates and TCP. Scale bar represents 100 μm.

fluorescence microscope (DM IL, Leica) [42].

2.8. Alkaline phosphatase (ALP) activity

Intracellular ALP activity of osteoblasts was investigated by using Alkaline Phosphatase Activity Colorimetric Assay Kit (Biovision Research Products) according to the manufacturer's instructions. After days 3, 7, and 14 of incubation, cells were rinsed with PBS and immediately frost at −80 °C. Following two freeze-thaw cycles, the cell suspension was centrifuged at 13,000 rpm for 10 min to remove supernatant. Then, cells were resuspended with assay buffer of the kit, and 5 mM p-nitrophenyl phosphate was added to each sample. After incubation for 60 min. at dark, stop solution was added to terminate ALP activity, and the absorbance values were recorded at 405 nm and calculated according to the standard curve by using the ALP enzyme of the assay kit.

2.9. Alizarin red staining

To observe the characteristic calcium deposition, a well-known alizarin red staining protocol was performed. In a typical staining, cells at days 7, 14, and 21 were washed with PBS and fixed in 4 % formaldehyde solution for 10 min. Then cells were rinsed with PBS and distilled water, followed by incubation in 2 % alizarin red solution (pH 4.2) for 20 min. Cells were rinsed with distilled water, and images were taken *via* optical microscopy [43].

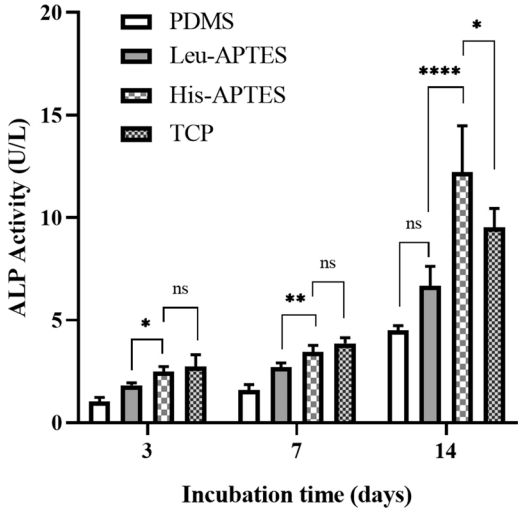

Fig. 5. ALP activity (U/L) of hFOB cells on native, Leu-APTES and His-APTES modified PDMS with positive control of TCP at different incubation times. Data were given as means ± SD and $n = 5$. Statistical significance values were calculated for each day, *$p < 0.05$, **$p < 0.01$, and ****$p < 0.0001$ (All groups were statistically significant relative to native PDMS with ****$p < 0.0001$, each day, except for Leu-APTES on Day 3, **$p < 0.01$).

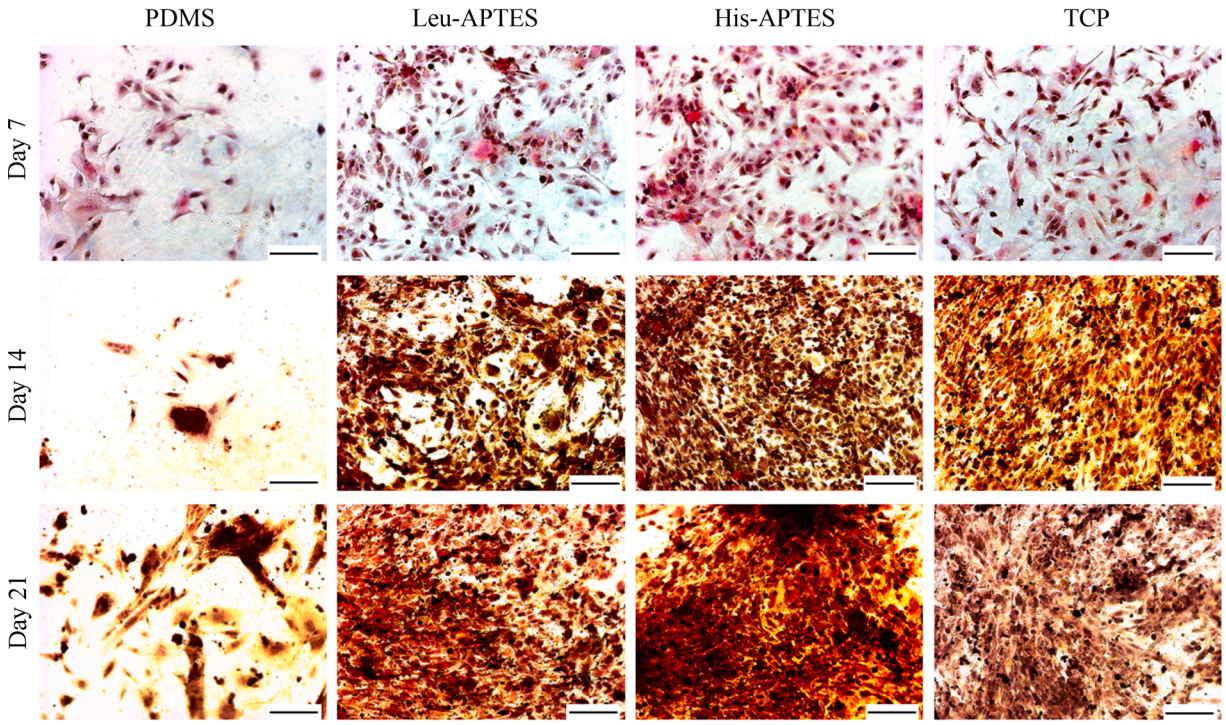

Fig. 6. Alizarin red staining of hFOB cells on native, Leu-APTES, and His-APTES modified PDMS with positive control of TCP at different incubation times. Scale bar represents 200 μm.

2.10. Statistical analysis

All of the results were reported as the mean ± standard deviation. Statistical differences between experimental groups were calculated by using one-way analysis of variance (ANOVA) followed by Tukey test. $p < 0.05$ was considered as being statistically significant.

3. Results and discussion

3.1. Analysis of Leu-APTES and His-APTES synthesis

^{1}H NMR data of the molecules are identical to our previous results [38]. In ^{1}H NMR data, recorded two doublet signals at around 8.25 ppm and two triplet signals around 7.60–7.80 ppm for Cbz-L-Leu-Bt and Cbz-L-His-Bt are characteristic signals for N-acylbenzotriazoles. These signals support the presence of benzotriazole in structure. After the reaction of APTES with benzotriazole functionalized intermediates, benzotriazole signals were disappeared. Thus, one can conclude that benzotriazole was substituted with the amino groups. Amide signal for Cbz-L-Leu-APTES was recorded at 7.24 ppm and 6.80 ppm for Cbz-L-His-APTES, respectively. On the other hand, characteristic methylene (−CH_2-) singlet signal recorded at around 5.10 ppm supports the presence of Cbz-protecting group. Another characteristic signal is methylene (−CH_2-) signal, which is bonded to silicon atom in APTES. This signal is generally recorded at around 0.50−0.60 ppm because of Si-C bonding. Finally, after deprotection of Cbz-group characteristic multiplet signal at around 7.30–7.40 ppm and singlet signal around 5.00 ppm for Cbz-moiety were disappeared. Additionally, broad signal around 4.20 ppm supports presence of free –NH_2 group of amino acids.

^{1}H NMR for L-His-APTES ($CDCl_3$ with 0.05 % v/v TMS, 500 MHz,): δ 10.15 (broad, s, 1H, N**H** imidazole), 7.50 (s, 1H, Ar-**H** imidazole), 6.92 (s, 1H, Ar-**H** imidazole), 6.79 (s, 1H, amide N**H**), 4.55−4.43 (m, 1H, -C**H**-NH_2), 4.23 (broad, s, 2H, -N**H$_2$**), 3.83 (q, J=6.90 Hz, 6H, OC**H$_2$**CH_3), 3.32−3.21 (m, 2H, −CONH-C**H$_2$**-), 3.12 (broad, s, 1H, CH-C**H$_2$**-imidazole), 2.98 (dd, J = 14,16, 5.00 Hz, 1H, CH-C**H$_2$**-imidazole), 1.62-1.44 (m, 2H, -CH_2-C**H$_2$**-CH_2-), 1.25 (t, J=8.27 Hz, 9H, OCH_2C**H$_3$**), 0.51-0.40 [m, 2H, -C**H$_2$**-Si(OEt_3)] ppm.

^{1}H NMR for L-Leu-APTES ($CDCl_3$ with 0.05 % v/v TMS, 500 MHz,): δ 7.24 (s, 1H, amide N**H**-), 4.25 (broad, s, 2H, -N**H$_2$**), 4.15 (dd, J = 8.29, 4.88 Hz, 1H, –C**H**-NH_2), 3.85 (q, J=6.98 Hz, 6H, OC**H$_2$**CH_3), 3.28 (dt, J = 11.92, 6.35 Hz, 2H, −CONH-C**H$_2$**CH_2-), 1.72−1.60 (m, 2H, −CH_2-C**H$_2$**−CH_2-), 1.55 (p, J=8.40 Hz, 2H, −CH_2-C**H$_2$**−CH_2-), 1.23 (t, J=6.98 Hz, 9H, OCH_2C**H$_3$**), 0.98−0.91 (m, 6H, −CH**(CH$_3$)$_2$**), 0.63 [t, J=8.00 Hz, 2H, -C**H$_2$**-Si(OEt_3)] ppm.

3.2. Self-assembly of Leu-APTES and His-APTES on PDMS substrates

Here we proposed a single step modification of PDMS with hydrophilic and hydrophobic amino acid conjugated SAMs. Characterization of surface chemistry was performed by XPS analysis and WCA measurements (Fig. 3). Oxygen plasma treatment was used to activate PDMS surfaces. Following this treatment, substrates were modified with increasing concentrations (1−20 mM) of His-APTES for 2 h to investigate the optimum conditions for the SAM formation. PDMS is a synthetic polymer, which is made up of silicon, carbon, oxygen, and hydrogen atoms [44]. Thus, modification of PDMS with His-APTES results in the presence of specific N1s signal in XPS spectra. Fig. 3A shows the high-resolution N1s core level overlay of PDMS substrates modified with increasing concentrations of His-APTES. From 1−5 mM His-APTES, the amount of nitrogen on substrate surface increases with increasing concentration, except for 10 mM, which provides the highest nitrogen content, and thereby the highest His-APTES coating of the surface. The decrease of N from 10−20 mM proves the maximum surface coverage was achieved with 10 mM and increasing the concentration caused the steric hindrance of imidazole rings. We propose that more molecules could not bind the surface with His-APTES concentration higher than 10 mM due to the shielding effect of the accessible functional groups on the surface. WCA measurements of His-APTES modified PDMS also prove the presence of hydrophilic histidine and exhibit a decreasing trend with increasing concentration (Fig. 3B). For the optimum dipping time investigation, 10 mM His-APTES solution was used to modify substrates with varying incubation ranges and XPS detection of N1s

shows that 24 h modification results in the highest nitrogen peak (Fig. 3C). Thus, 10 mM concentration and 24 h dipping time are considered to be the optimum modification parameters for both His-APTES and Leu-APTES and all experiments were performed accordingly.

Fig. 3E indicates the binding energies corresponding to O1s, C1s, Si2s, and Si2p PDMS-specific peaks at 532.8, 285.1, 154.0, and 102.7 eV were detected in all samples [44]. Besides, peaks at 401.1 eV appeared after Leu-APTES and His-APTES modifications, which were assigned to N1s core line [38]. Observation of these peaks in both modified substrate surfaces was a certain indication for the presence of the molecules on PDMS substrates. When compared between modified surfaces, the increase of N1s peak in His-APTES modified PDMS showed relatively higher surface nitrogen content of the surface, due to the extra nitrogen atoms in the imidazole ring of the molecule.

The quantitative elemental composition of native and modified substrates was summarized in Table 1. Compared to native PDMS, modification with Leu-APTES and His-APTES resulted in increased O% and N% with a concomitant decrease in Si%. Treatment with oxygen plasma prior to modification was responsible for the increase in oxygen content in both functionalized groups. The presence of N atom is an indication of SAMs modification, and the relation between theoretical and measured atomic percentages of N provides information about the surface coverage. In Leu-APTES group, the atomic percentage of N was expected to be 10.53 if the surface was fully covered, whereas XPS analysis shows that the surface N content was only 1.35 %. Thus, approximately 13 % of the surface is covered with Leu-APTES. Similarly, stoichiometric and measured values of N% in His-APTES modified PDMS are 19 and 2.96, respectively, giving a surface density of 16 %. Full surface coverage with SAMs may not be possible due to many issues: i) low surface densities (the number of activated surface functional groups), ii) the orientation of SAMs in a way to hinder accessible hydroxyl groups and iii) the repulsive forces between SAMs.

Water contact angles (WCA) of hydrophilic and hydrophobic amino acid conjugated SAMs modified PDMS substrate surfaces were utilized to confirm the alterations in surface wettability, as shown in Fig. 3F. In agreement with the literature, WCA of native PDMS was found in the hydrophobic region, which was measured to be $106.2 \pm 3.1^{\circ}$ [45]. After oxygen plasma treatment for 1 min, WCA was measured below 14° [46], showing the presence of Si—OH bonds. These bonds facilitated amino acid conjugated APTES modification of PDMS surfaces. After incorporation of Leu-APTES and His-APTES, very low WCA of plasma oxygenated PDMS was increased to $85.0 \pm 4.9^{\circ}$ and $43.5 \pm 5.3^{\circ}$, creating hydrophobic and hydrophilic surfaces, respectively. Previous studies documented the hydrophilic nature of APTES modified PDMS, which is a result of functional $—NH_2$ groups of the molecule [47]. Here, both His-APTES and Leu-APTES have these amino functional groups, and thereby both of these SAMs modification resulted in surfaces with hydrophilic properties, partially. Histidine is known as a hydrophilic amino acid with pH responsive characteristics due to its imidazole ring side chain [48] and in this study His-APTES modified PDMS demonstrated hydrophilic surfaces, as expected. The isoelectric point (p*I*) of histidine is 7.59, where p*Ka* value 3N-H of the imidazole ring is pH = 6.0. Below p*I*, the net charge of the histidine amino acid will be positive [49]. However, in this study, histidine is conjugated to the APTES molecule`s amino group through its carboxylic acid group. Due to the amide bond formation and loss of the acidic functional group (COOH), it is not possible to accurately calculate the p*I* of His-APTES molecules. Imidazole ring will be responsible for the protonation and deprotonation of the His-APTES molecule during SAM-cell interactions. In S1, pH responsibility of SAMs from His-APTES was investigated *via* zeta potential measurements and cationic methylene blue (MB) & anionic eosin y disodium salt (EY) adsorption study at different pH values (pH = 5.0, 7.4 and 9.0). Zeta potential measurements of His-APTES functionalized silica nanoparticles (SNPs) are given in Fig. S3. In the literature, it is very well-know that, nanoparticles having zeta potentials between −10 and +10 mV are regarded as approximately neutral, while nanoparticles are regarded to be strongly cationic and strongly anionic with greater zeta potentials than +30 mV or less zeta potentials than −30 mV, respectively [50]. According to the zeta potential analysis, SNPs exhibited a pH dependent trend like other nanoparticles; the more negative zeta potentials are obtained with increasing pH [51]. The zeta potential of SNPs at pH = 5.0 showed slightly positive charge, where His-APTES functionalization resulted strongly cationic SNP surfaces with an average zeta potential value of $+37.9 \pm 1.1$ mV. Similarly, surface charge of anionic SNP with an average zeta potential of -27.6 ± 0.9 mV at pH = 7.4 [52] was confirmed to be altered after His-APTES incorporation, which was found to be approximately neutral/slightly positive with an average zeta potential of $+8.6 \pm 0.6$ mV. SNPs at pH = 9.0 have the most strongly anionic surface charge among all others and yet SNPs modified with His-APTES resulted approximately neutral/slightly negatively charged particles. To sum up, at pH 7.4, His-APTES modified SNP have shown approximately neutral/slightly positive surface charge. This finding does not fully support the positively charged His-APTES molecules at pH = 7.4. The phenomena may be explained as zeta potential analysis were conducted by using SNPs instead of PDMS surfaces and aggregation of these nanoparticles may affect the given results. Also, these findings at pH 7.4 may not represent the actual cell culture environment. In general, cell culture studies were performed at pH = 7.4, however pH of the medium could decrease to more acidic pH values due to metabolic activity of cells and possible cell debris. Under these conditions, imidazole side chain carrying unpaired electrons can bind a proton reversibly to make the molecule partially positively charged. For clarification of this point, cationic MB and anionic EY adsorption study was also conducted to clarify zeta potential measurements by using directly His-APTES modified PDMS surfaces. Fig. S4 shows the amount of MB and EY dyes adsorbed (Q, μg) on His-APTES modified PDMS. At pH = 5.0, His-APTES modified PDMS showed the weakest adsorption for cationic MB, due the repulsive forces between dye cations and positively charged His-APTES molecules on the PDMS surface; where a slight decrease in the positive charge was expressed at pH = 7.4, and at pH = 9.0 the highest adsorption capacity was obtained (due to the increased number of negative charges on His-APTES modified PDMS surface). Furthermore, the anionic EY dye adsoption study also confirmed the positively charged His-APTES molecules on the PDMS surface *via* electrostatic interactions. Surface charge of His-APTES modified PDMS at pH = 5.0 and 7.4 was considered to be positive, as anionic EY adsorption capacity at these pHs were found to be higher than pH = 9.0. The lowest amount of EY adsorption was found on surfaces at pH = 9.0, which demonstrates the decrease in the positive surface charge. Here, the pH sensitivity of His-APTES modified PDMS surface's charge is clearly shown and the change in the surface charge is found to be not as sensitive to pH as histidine amino acid [48,49]. Zeta potential measurements, together with MB & EY adsorption study confirmed the stability of positively charged His-APTES and related hydrophilic nature of His-APTES modified PDMS at physiological pH and cell culture conditions. In contrast, hydrophobic leucine amino acid conjugated SAMs modification leads to an increased WCA value that fell into the hydrophobic region [53].

The stability of SAMs modification was confirmed under constant flow regime for different time duration *via* XPS analyses and WCA measurements (SI). Fig. S2.A shows the XPS survey spectra of His-APTES modified PDMS surfaces under flow for 0.5 and 4 h with a control group. All His-APTES modified PDMS–related peaks corresponding to O1s, N1s, C1s, Si2s and Si2p were detected in all groups with no significant differences between the signal intensities. Furthermore, similar atomic percentages of N atom in all experimental groups are a direct evidence for stable His-APTES modification, regardless of applied flow for different duration. The standard deviation between measured N atomic percentages of His-APTES modified PDMS before or after constant flow was calculated as ± 0.08 %. Supporting the XPS analyses, WCA measurements of His-APTES modified PDMS surfaces (Fig. S2.B) shows no

statistically significant differences according to applied flow. APTES modification is a well-known procedure and has been used in many applications to provide stable linkages under load or pressure; in microfluidics, introducing biomolecules for cell substrates, altering wettability properties, *etc.* Atomic Force Microscopy (AFM) is one of the techniques to confirm the long term APTES linkage supported stability of surface modification inside a microfluidic system under various flow rates and continuous flow at different shear stresses [54]. Specific properties of immobilized molecules (like enzymatic activity) have also used to verify APTES linkage supported stability for long term [55]. As the modification of PDMS substrates were completed through APTES based chemistry, amino acid SAMs modified surfaces are stable under flow, similar to the examples given above, PDMS surface keeps its stability under a constant and continuous flow regime at least up to 4 h, which is a critical time point for initial cell adhesion [56], make these modifications suitable for cell culture studies.

3.3. Cell proliferation on PDMS substrates

Cytocompatibility and proliferation of amino acid conjugated SAMs modification on PDMS substrates were evaluated by *in vitro* hFOB cell culture. Cells were cultured on native and modified substrates and incubated for 7 days. On days 1, 3, and 7 of cell culture, the metabolic activity of the cells was determined using Alamar blue assay, which provides repeated investigation of the same samples. Fig. 4A shows the reduced Alamar blue percentages relative to the cell proliferation on amino acid conjugated SAMs modified PDMS, native PDMS, and Tissue Culture Polystyrene (TCP), as a positive control. The increase in the reduced Alamar blue percentage indicates the proliferation of cells on substrates. According to the results, cells in all experimental groups were remained viable and also in a tendency of growth in time, confirming the non-toxic nature of PDMS. Furthermore, cells on His-APTES modified PDMS affects proliferation in a similar way to TCP. For the whole culture period, both Leu-APTES and His-APTES modification improved the metabolic activity of cells significantly, when compared with the native PDMS. The analysis indicated that cells on both hydrophilic and hydrophobic SAMs modified substrates were healthy and viable without any significant difference after day 3 of incubation, suggesting all modifications provided sufficient bioactivity. Increased cell proliferation on His-APTES can be attributed to surface hydrophilicity [57], but using a relatively hydrophobic molecule, Leu-APTES, could also have increased cellular metabolic activity for short time, due to its biomimetic nature. Besides, amino and carboxylic acid groups of Leu-APTES provide partially hydrophilic regions to these molecules, which could also be the reason for the enhanced expansion of the cells.

After day 3, the number of viable cells was increased distinctively on His-APTES modified surfaces. This significant increase starting from day 3 of incubation showed that the wettability of surfaces influences cellular metabolic activity in long periods periods and also it confirmed the impact of hydrophilicity on improved osteoblast behavior and growth, leading to increased cellular proliferation [58]. Apart from being a hydrophilic amino acid, histidine is also one of the amino acids in FHRRIKA peptide sequence, which is a heparin-binding domain of bone sialoprotein [59]. Stile et al. documented that modification of hydrogels with this histidine-containing peptide enhanced proliferation and spreading of rat calvarial osteoblasts [60]. In another study with rat calvarial osteoblasts performed by Schuler et al., the enhanced proliferation of cells on FHRRIKA peptide-modified titanium was showed [61].

3.4. Actin cytoskeleton organization

Actin cytoskeleton organization of hFOB cells on PDMS substrates was investigated to show cellular morphology by dual fluorescent staining of Alexa Fluor 488-phalloidin and DAPI, 7 days post-seeding. As shown in Fig. 4B, modification of PDMS surface with both SAMs resulted in enhanced interactions. Only a few adhered cells were observed on native PDMS substrates as well as cells exhibiting poorly developed actin stress fibers, which might associate to the hydrophobic nature of the material [62]. The aggregate formation was occurred as a reason for decreased cell attachment, supporting the low number of living cells found in Alamar blue assay. This response of hFOBs on hydrophobic surfaces was compatible with the literature [42,63]. Leu-APTES modification of PDMS also resulted in relatively hydrophobic surface, but cells on these substrates were higher in number and showed better attachment than native PDMS, even though actin bundles of cells were short and disrupted. On the other hand, cells on hydrophilic His-APTES modified PDMS substrates exhibit a multilayer morphology, similar to cells on TCP, with well-defined and high number of actin fibers linking adjacent cells [64]. Similar effect of surface hydrophilicity on osteoblasts was documented by Toffoli et al. They reported that thermally-induced hydrophilicity of titanium substrates enhanced actin cytoskeleton organization of MC3T3-E1 pre-osteoblast cells [33]. Furthermore, a distinctive spindle-like morphology of cells was exhibited on both of His-APTES and TCP. These features may be contributed to sign of osteogenic maturation [36]. Thus, surface hydrophilicity, in addition to different amino acid biochemistry, can impact substrate surface-osteoblast cell interaction in means of attachment and cellular extension.

3.5. ALP activity

Alkaline phosphatase is an early osteogenic marker which regulates bone-specific extracellular matrix mineralization [65]. hFOB cells are osteoblast precursors, and the increase in the ALP expression is an indication of a mature osteoblastic phenotype [66,67]. Thus, osteoblastic behavior of hFOBs on PDMS substrates was investigated from the ALP activity for 14 days. As seen in Fig. 5, ALP activity of cells on all substrates showed an ascending trend from day 3 to day 14. There was a significant increase in both SAMs modified surfaces relative to native PDMS until day 14. This trend is similar to the findings of Jones et al., where they documented the highest ALP activity of human osteoblasts on day 14 [68]. Throughout the culture period, His-APTES modified PDMS resulted in significantly higher ALP production when compared to native and Leu-APTES modified PDMS. An increase in the ALP activity was observed, especially when hydrophilic functional groups are higher on substrate surfaces [36]. Although Leu-APTES modified PDMS showed relatively hydrophobic surface properties, -NH_2 and $-CH_3$ functional groups of the molecule enabled enhanced osteogenic behavior when compared with native PDMS until day 14 [29]. His-APTES modified surfaces and control group, TCP, showed similar effects on cells with no significant differences until day 7, and on day 14 cells on His-APTES modified PDMS exhibited higher ALP activity than TCP ($p < 0.05$). The trend was agreed with the proliferation results and cytoskeleton organization of cells, as the increase in cell number was the highest in His-APTES and TCP groups until day 7. The increase in proliferation and accumulation of osteoblasts provokes cell maturation and accordingly ALP activity [62]. Fig. 5 shows that cells on PDMS substrates reached confluence after day 7 and thus accumulation of cells, especially on hydrophilic His-APTES modified PDMS, promoted osteogenesis of hFOBs, confirmed the effect of wettability [69] in accordance to higher cell numbers on osteogenic differentiation [70].

3.6. Alizarin red staining

Alizarin red staining is an indicator of calcium depositions in extracellular matrix [71]. Optical images of native and modified PDMS surfaces after alizarin red staining were depicted in Fig. 6. As seen in the figure, subsequently from day 7–21, alizarin red staining was shown to be denser in all groups. Compatible with the ALP activity results, cell expansion and accumulation enabled them to progress into osteoblastic growth period after day 7 of culture on the substrates. After this day,

ECM mineralization was accelerated [72]. The effect of surface modification on osteoblastic phenotype was supported here one more time, where on modified groups higher intensity of staining was recorded. Leu-APTES modified PDMS cells did not provide significantly increased ALP activity (relative to native PDMS) on day 14, however alizarin staining on the same day showed better osteogenic behavior than cells on native PDMS. Moreover, Leu-APTES modified PDMS leads to similar calcium deposition to TCP, thanks to its biomimetic functional groups [29]. Cells on His-APTES modified PDMS displayed a qualitatively higher amount of matrix mineralization among all groups for all time points. Especially on day 21, cells exhibited classical mineralization nodules and increased intensity of color with higher cell density. Biomineralization is an indicator of osteogenic efficacy and bone formation [73]. Here, the presence of qualitatively more calcium deposition of cells on His-APTES than other experimental groups is consistent with the other osteogenic marker, ALP activity, and proves that hFOBs on His-APTES modified PDMS differentiated enough to deposit higher amount of mineralized ECM than that of control group, TCP [65]. These ALP activity and calcium deposition overall results demonstrated the combination of a biomimetic and hydrophilic modification's superior effect on PDMS surfaces for *in vitro* osteoblast cell culture and maturation.

4. Conclusions

Hydrophilic and hydrophobic amino acid conjugated SAMs were prepared, and surface modification with these molecules was investigated to improve cell-substrate surface characteristics of PDMS for long-term osteoblast cell culture. Optimum surface modification parameters with these SAMs were found to be 10 mM concentration and 24 h dipping time, by using the highest nitrogen content in high-resolution N1s spectra of XPS and complementary WCA measurements. Both modified surfaces provided cell proliferation and maturation; however, in the latter times of culture, hydrophilic His-APTES facilitated a superior osteoblastic behavior than the positive control, TCP. Surprisingly, Leu-APTES functionalization provides a significantly improved cell response respect to native PDMS, even though they both showed a hydrophobic nature. Herein, we suggested that biomimetic modification has predominant effects on cells than the wettability of the surfaces. Moreover, His-APTES and Leu-APTES provided a supportive environment to hFOB cells for three weeks of culture, proving that modification stability could be preserved with SAMs for at least three weeks. This biomimetic and straightforward surface modification of PDMS is a promising technique to enhance bone cell - substrate interactions that may be used in *in vitro* cell culture studies, regenerative medicine applications as well as microfluidic systems.

CRediT authorship contribution statement

M. Özgen Öztürk-Öncel: Conceptualization, Methodology, Data curation, Writing - original draft. **Sedat Odabaş:** Writing - review & editing. **Lokman Uzun:** Writing - review & editing. **Deniz Hür:** Writing - review & editing. **Bora Garipcan:** Resources, Funding acquisition, Supervision, Writing - review & editing.

Declaration of Competing Interest

The authors declare that they have no known competing financial interests or personal relationships that could have appeared to influence the work reported in this paper.

Acknowledgments

This study was supported by TUBITAK (Grant No. 112T564) and Bogazici University Research Fund (Grant No: 6701).

Appendix A. Supplementary data

Supplementary material related to this article can be found, in the online version, at doi:https://doi.org/10.1016/j.colsurfb.2020.111343.

References

[1] Y.J. Chuah, Z.T. Heng, J.S. Tan, L.M. Tay, C.S. Lim, Y. Kang, D.A. Wang, Surface modifications to polydimethylsiloxane substrate for stabilizing prolonged bone marrow stromal cell culture, Colloids Surf. B Biointerfaces (2020), https://doi.org/10.1016/j.colsurfb.2020.110995.
[2] J. Fu, Y.J. Chuah, J. Liu, S.Y. Tan, D.A. Wang, Respective effects of gelatin-coated polydimethylsiloxane (PDMS) substrates on self-renewal and cardiac differentiation of induced pluripotent stem cells (iPSCs), ACS Biomater. Sci. Eng. (2018), https://doi.org/10.1021/acsbiomaterials.8b00993.
[3] Y. Poojari, Silicones for Encapsulation of Medical Device Implants, Silicon, 2017, https://doi.org/10.1007/s12633-017-9603-4.
[4] C. Hassler, T. Boretius, T. Stieglitz, Polymers for neural implants, J. Polym. Sci. Part B Polym. Phys. (2011), https://doi.org/10.1002/polb.22169.
[5] W.F. Quirós-Solano, N. Gaio, O.M.J.A. Stassen, Y.B. Arik, C. Silvestri, N.C.A. Van Engeland, A. Van der Meer, R. Passier, C.M. Sahlgren, C.V.C. Bouten, A. van den Berg, R. Dekker, P.M. Sarro, Microfabricated tuneable and transferable porous PDMS membranes for Organs-on-Chips, Sci. Rep. (2018), https://doi.org/10.1038/s41598-018-31912-6.
[6] J. El-Ali, P.K. Sorger, K.F. Jensen, Cells on chips, Nature (2006), https://doi.org/10.1038/nature05063.
[7] C. Wei, B. Fan, D. Chen, C. Liu, Y. Wei, B. Huo, L. You, J. Wang, J. Chen, Osteocyte culture in microfluidic devices, Biomicrofluidics (2015), https://doi.org/10.1063/1.4905692.
[8] P.S. Dittrich, A. Manz, Lab-on-a-chip: microfluidics in drug discovery, Nat. Rev. Drug Discov. (2006), https://doi.org/10.1038/nrd1985.
[9] A. Mata, A.J. Fleischman, S. Roy, Characterization of polydimethylsiloxane (PDMS) properties for biomedical micro/nanosystems, Biomed. Microdevices (2005), https://doi.org/10.1007/s10544-005-6070-2.
[10] I. Wong, C.M. Ho, Surface molecular property modifications for poly (dimethylsiloxane) (PDMS) based microfluidic devices, Microfluid. Nanofluidics (2009), https://doi.org/10.1007/s10404-009-0443-4.
[11] H. Hillborg, N. Tomczak, A. Olàh, H. Schönherr, G.J. Vancso, Nanoscale hydrophobic recovery: a chemical force microscopy study of UV/ozone-treated cross-linked poly(dimethylsiloxane), Langmuir (2004), https://doi.org/10.1021/la035552k.
[12] H. Hillborg, U.W. Gedde, Hydrophobicity recovery of polydimethylsiloxane after exposure to corona discharges, Polymer (Guildf) (1998), https://doi.org/10.1016/S0032-3861(97)00484-9.
[13] T. Senzai, S. Fujikawa, Fast hydrophobicity recovery of the surface-hydrophilic poly(dimethylsiloxane) films caused by rechemisorption of dimethylsiloxane derivatives, Langmuir 35 (2019) 9747–9752, https://doi.org/10.1021/acs.langmuir.9b01448.
[14] G.G. Genchi, G. Ciofani, I. Liakos, L. Ricotti, L. Ceseracciu, A. Athanassiou, B. Mazzolai, A. Menciassi, V. Mattoli, Bio/non-bio interfaces: a straightforward method for obtaining long term PDMS/muscle cell biohybrid constructs, Colloids Surf. B Biointerfaces (2013), https://doi.org/10.1016/j.colsurfb.2012.12.035.
[15] C.J. Pan, H. Qin, Y.D. Nie, H.Y. Ding, Control of osteoblast cells adhesion and spreading by microcontact printing of extracellular matrix protein patterns, Colloids Surf. B Biointerfaces (2013), https://doi.org/10.1016/j.colsurfb.2012.11.045.
[16] S. Kuddannaya, Y.J. Chuah, M.H.A. Lee, N.V. Menon, Y. Kang, Y. Zhang, Surface chemical modification of poly(dimethylsiloxane) for the enhanced adhesion and proliferation of mesenchymal stem cells, ACS Appl. Mater. Interfaces (2013), https://doi.org/10.1021/am402903e.
[17] Y.J. Chuah, Y.T. Koh, K. Lim, N.V. Menon, Y. Wu, Y. Kang, Simple surface engineering of polydimethylsiloxane with polydopamine for stabilized mesenchymal stem cell adhesion and multipotency, Sci. Rep. (2015), https://doi.org/10.1038/srep18162.
[18] S. Kuddannaya, J. Bao, Y. Zhang, Enhanced in vitro biocompatibility of chemically modified poly(dimethylsiloxane) surfaces for stable adhesion and long-term investigation of brain cerebral cortex cells, ACS Appl. Mater. Interfaces (2015), https://doi.org/10.1021/acsami.5b09032.
[19] Z. Yue, X. Liu, P.J. Molino, G.G. Wallace, Bio-functionalisation of polydimethylsiloxane with hyaluronic acid and hyaluronic acid - collagen conjugate for neural interfacing, Biomaterials 32 (2011) 4714–4724, https://doi.org/10.1016/j.biomaterials.2011.03.032.
[20] N.S. Bhairamadgi, S.P. Pujari, F.G. Trovela, A. Debrassi, A.A. Khamis, J.M. Alonso, A.A. Al Zahrani, T. Wennekes, H.A. Al-Turaif, C. Van Rijn, Y.A. Alhamed, H. Zuilhof, Hydrolytic and thermal stability of organic monolayers on various inorganic substrates, Langmuir (2014), https://doi.org/10.1021/la500533f.
[21] A. Hasan, S.K. Pattanayek, L.M. Pandey, Effect of functional groups of self-assembled monolayers on protein adsorption and initial cell adhesion, ACS Biomater. Sci. Eng. 4 (2018) 3224–3233, https://doi.org/10.1021/acsbiomaterials.8b00795.
[22] A. Hasan, L.M. Pandey, Surface modification of Ti6Al4V by forming hybrid self-assembled monolayers and its effect on collagen-I adsorption, osteoblast adhesion and integrin expression, Appl. Surf. Sci. (2019), https://doi.org/10.1016/j.apsusc.2019.144611.

[23] G. Mani, D.M. Johnson, D. Marton, M.D. Feldman, D. Patel, A.A. Ayon, C. M. Agrawal, Drug delivery from gold and titanium surfaces using self-assembled monolayers, Biomaterials (2008), https://doi.org/10.1016/j.biomaterials.2008.08.014.

[24] J.M. Alonso, A.A.M. Bielen, W. Olthuis, S.W.M. Kengen, H. Zuilhof, M.C. R. Franssen, Self-assembled monolayers of 1-alkenes on oxidized platinum surfaces as platforms for immobilized enzymes for biosensing, Appl. Surf. Sci. (2016), https://doi.org/10.1016/j.apsusc.2016.05.006.

[25] A. Nanci, J.D. Wuest, L. Peru, P. Brunet, V. Sharma, S. Zalzal, M.D. McKee, Chemical modification of titanium surfaces for covalent attachment of biological molecules, J. Biomed. Mater. Res. (1998), https://doi.org/10.1002/(SICI)1097-4636(199805)40:2<324::AID-JBM18>3.0.CO;2-L.

[26] L.M. Pandey, S.K. Pattanayek, Hybrid surface from self-assembled layer and its effect on protein adsorption, Appl. Surf. Sci. (2011), https://doi.org/10.1016/j.apsusc.2010.12.148.

[27] N. Marín-Pareja, M. Cantini, C. González-García, E. Salvagni, M. Salmerón-Sánchez, M.P. Ginebra, Different organization of type I collagen immobilized on silanized and nonsilanized titanium surfaces affects fibroblast adhesion and fibronectin secretion, ACS Appl. Mater. Interfaces (2015), https://doi.org/10.1021/acsami.5b05420.

[28] B.G. Keselowsky, D.M. Collard, A.J. García, Integrin binding specificity regulates biomaterial surface chemistry effects on cell differentiation, Proc. Natl. Acad. Sci. U. S. A. (2005), https://doi.org/10.1073/pnas.0407356102.

[29] J.M. Curran, R. Chen, J.A. Hunt, The guidance of human mesenchymal stem cell differentiation in vitro by controlled modifications to the cell substrate, Biomaterials (2006), https://doi.org/10.1016/j.biomaterials.2006.05.001.

[30] B. Cao, Y. Peng, X. Liu, J. Ding, Effects of functional groups of materials on nonspecific adhesion and chondrogenic induction of mesenchymal stem cells on free and micropatterned surfaces, ACS Appl. Mater. Interfaces 9 (2017) 23574–23585, https://doi.org/10.1021/acsami.7b08339.

[31] M. Padial-Molina, P. Galindo-Moreno, J.E. Fernández-Barbero, F. O'Valle, A. B. Jódar-Reyes, J.L. Ortega-Vinuesa, P.J. Ramón-Torregrosa, Role of wettability and nanoroughness on interactions between osteoblast and modified silicon surfaces, Acta Biomater. (2011), https://doi.org/10.1016/j.actbio.2010.08.024.

[32] R.A. Gittens, R. Olivares-Navarrete, A. Cheng, D.M. Anderson, T. McLachlan, I. Stephan, J. Geis-Gerstorfer, K.H. Sandhage, A.G. Fedorov, F. Rupp, B.D. Boyan, R. Tannenbaum, Z. Schwartz, The roles of titanium surface micro/nanotopography and wettability on the differential response of human osteoblast lineage cells, Acta Biomater. (2013), https://doi.org/10.1016/j.actbio.2012.12.002.

[33] A. Toffoli, L. Parisi, M.G. Bianchi, S. Lumetti, O. Bussolati, G.M. Macaluso, Thermal treatment to increase titanium wettability induces selective proteins adsorption from blood serum thus affecting osteoblasts adhesion, Mater. Sci. Eng. C. (2020), https://doi.org/10.1016/j.msec.2019.110250.

[34] Y. Arima, H. Iwata, Effect of wettability and surface functional groups on protein adsorption and cell adhesion using well-defined mixed self-assembled monolayers, Biomaterials (2007), https://doi.org/10.1016/j.biomaterials.2007.03.013.

[35] M.T. Conconi, M. Tommasini, E. Muratori, P.P. Parnigotto, Essential amino acids increase the growth and alkaline phosphatase activity in osteoblasts cultured in vitro, Farmaco (2001), https://doi.org/10.1016/S0014-827X(01)01126-0.

[36] Y. Xiong, J. Huang, L. Fu, H. Ren, S. Li, W. Xia, Y. Yan, Enhancement of osteoblast cells osteogenic differentiation and bone regeneration by hydroxyapatite/phosphoester modified poly(amino acid), Mater. Sci. Eng. C. 111 (2020), 110769, https://doi.org/10.1016/j.msec.2020.110769.

[37] A. Cattoni, J. Chen, D. Decanini, J. Shi, A.-M. Haghiri-Gosnet, Soft UV Nanoimprint Lithography: A Versatile Tool for Nanostructuration at the 20nm Scale, in: Recent Adv, Nanofabrication Tech. Appl. (2011), https://doi.org/10.5772/21874.

[38] A.R. Katritzky, P. Angrish, D. Hür, K. Suzuki, N-(Cbz- and Fmoc-α-aminoacyl) benzotriazoles: Stable derivatives enabling peptide coupling of Tyr, Trp, Cys, Met, and Gln with free amino acids in aqueous media with complete retention of chirality, Synthesis (Stuttg) (2005), https://doi.org/10.1055/s-2005-861782.

[39] C.K. Akkan, D. Hür, L. Uzun, B. Garipcan, Amino acid conjugated self assembling molecules for enhancing surface wettability of fiber laser treated titanium surfaces, Appl. Surf. Sci. (2016), https://doi.org/10.1016/j.apsusc.2016.01.083.

[40] P.J. Wipff, H. Majd, C. Acharya, L. Buscemi, J.J. Meister, B. Hinz, The covalent attachment of adhesion molecules to silicone membranes for cell stretching applications, Biomaterials (2009), https://doi.org/10.1016/j.biomaterials.2008.12.022.

[41] G.B. Ateş, A. Ak, B. Garipcan, M. Gülsoy, Indocyanine green-mediated photobiomodulation on human osteoblast cells, Lasers Med. Sci. (2018), https://doi.org/10.1007/s10103-018-2530-9.

[42] R.A. D'Sa, J. Raj, P.J. Dickinson, F. McCabe, B.J. Meenan, Human fetal osteoblast response on poly(Methyl methacrylate)/Polystyrene demixed thin film blends: surface chemistry vs topography effects, ACS Appl. Mater. Interfaces 8 (2016) 14920–14931, https://doi.org/10.1021/acsami.5b08073.

[43] Y. Zhu, Z. Cao, Y. Peng, L. Hu, T. Guney, B. Tang, Facile surface modification method for synergistically enhancing the biocompatibility and bioactivity of poly (ether ether ketone) that induced osteodifferentiation, ACS Appl. Mater. Interfaces (2019), https://doi.org/10.1021/acsami.9b03030.

[44] X.H. Qin, B. Senturk, J. Valentin, V. Malheiro, G. Fortunato, Q. Ren, M. Rottmar, K. Maniura-Weber, Cell-Membrane-Inspired Silicone Interfaces that Mitigate Proinflammatory Macrophage Activation and Bacterial Adhesion, Langmuir (2019), https://doi.org/10.1021/acs.langmuir.8b02292.

[45] T. Senzai, S. Fujikawa, Fast hydrophobicity recovery of the surface-hydrophilic poly(dimethylsiloxane) films caused by rechemisorption of dimethylsiloxane derivatives, Langmuir 35 (2019) 9747–9752, https://doi.org/10.1021/acs.langmuir.9b01448.

[46] Y. Zhao, J. Wen, Y. Ge, X. Zhang, H. Shi, K. Yang, X. Gao, S. Shi, Y. Gong, Fabrication of stable biomimetic coating on PDMS surface: cooperativity of multivalent interactions, Appl. Surf. Sci. (2019), https://doi.org/10.1016/j.apsusc.2018.11.056.

[47] Y.J. Chuah, S. Kuddannaya, M.H.A. Lee, Y. Zhang, Y. Kang, The effects of poly (dimethylsiloxane) surface silanization on the mesenchymal stem cell fate, Biomater. Sci. (2015), https://doi.org/10.1039/c4bm00268g.

[48] Z. Tu, A. Young, C. Murphy, J.F. Liang, The pH sensitivity of histidine-containing lytic peptides, J. Pept. Sci. (2009), https://doi.org/10.1002/psc.1180.

[49] M.K. Campbell, S.O. Farrel, Biochemistry. Cengage Learning, 7th ed., 2012, pp. 69–70.

[50] J.D. Clogston, A.K. Patri, Zeta potential measurement, Methods Mol. Biol. (2011), https://doi.org/10.1007/978-1-60327-198-1_6.

[51] K.M. Kim, H.M. Kim, W.J. Lee, C.W. Lee, T. Il Kim, J.K. Lee, J. Jeong, S.M. Paek, J. M. Oh, Surface treatment of silica nanoparticles for stable and charge-controlled colloidal silica, Int. J. Nanomedicine (2014), https://doi.org/10.2147/IJN.S57922.

[52] H.I. Alkhammash, N. Li, R. Berthier, M.R.R. De Planque, Native silica nanoparticles are powerful membrane disruptors, Phys. Chem. Chem. Phys. (2015), https://doi.org/10.1039/c4cp05882h.

[53] M. Lointier, C. Aisenbrey, A. Marquette, J.H. Tan, A. Kichler, B. Bechinger, Membrane pore-formation correlates with the hydrophilic angle of histidine-rich amphipathic peptides with multiple biological activities, Biochim. Biophys. Acta Biomembr. (2020), 183212, https://doi.org/10.1016/j.bbamem.2020.183212.

[54] A. Siddique, T. Meckel, R.W. Stark, S. Narayan, Improved cell adhesion under shear stress in PDMS microfluidic devices, Colloids Surf. B Biointerfaces (2017), https://doi.org/10.1016/j.colsurfb.2016.11.011.

[55] F.M. Hernández-Maya, M.P. Cañizares-Macías, Evaluation of the activity of β-glucosidase immobilized on polydimethylsiloxane (PDMS) with a microfluidic flow injection analyzer with embedded optical fibers, Talanta (2018), https://doi.org/10.1016/j.talanta.2018.03.038.

[56] X. Liu, J.Y. Lim, H.J. Donahue, R. Dhurjati, A.M. Mastro, E.A. Vogler, Influence of substratum surface chemistry/energy and topography on the human fetal osteoblastic cell line hFOB 1.19: phenotypic and genotypic responses observed in vitro, Biomaterials (2007), https://doi.org/10.1016/j.biomaterials.2007.06.016.

[57] S.Y. Yang, E.S. Kim, G. Jeon, K.Y. Choi, J.K. Kim, Enhanced adhesion of osteoblastic cells on polystyrene films by independent control of surface topography and wettability, Mater. Sci. Eng. C. (2013), https://doi.org/10.1016/j.msec.2012.12.081.

[58] C. Fu, X. Yang, S. Tan, L. Song, Enhancing cell proliferation and osteogenic differentiation of MC3T3-E1 pre-osteoblasts by BMP-2 delivery in graphene oxide-incorporated PLGA/HA biodegradable microcarriers, Sci. Rep. (2017), https://doi.org/10.1038/s41598-017-12935-x.

[59] I. Pountos, M. Panteli, A. Lampropoulos, E. Jones, G.M. Calori, P.V. Giannoudis, The role of peptides in bone healing and regeneration: a systematic review, BMC Med. (2016), https://doi.org/10.1186/s12916-016-0646-y.

[60] R.A. Stile, K.E. Healy, Thermo-responsive peptide-modified hydrogels for tissue regeneration, Biomacromolecules (2001), https://doi.org/10.1021/bm0000945.

[61] M. Schuler, D.W. Hamilton, T.P. Kunzler, C.M. Sprecher, M. De Wild, D. M. Brunette, M. Textor, S.G.P. Tosatti, Comparison of the response of cultured osteoblasts and osteoblasts outgrown from rat calvarial bone chips to nonfouling KRSR and FHRRIKA-peptide modified rough titanium surfaces, J. Biomed. Mater. Res. - Part B Appl. Biomater. (2009), https://doi.org/10.1002/jbm.b.31425.

[62] B. Liu, L. Chen, C. Shao, F. Zhang, K. Zhou, J. Cao, D. Zhang, Improved osteoblasts growth on osteomimetic hydroxyapatite/BaTiO3 composites with aligned lamellar porous structure, Mater. Sci. Eng. C. 61 (2016) 8–14, https://doi.org/10.1016/j.msec.2015.12.009.

[63] J.Y. Lim, A.F. Taylor, Z. Li, E.A. Vogler, H.J. Donahue, Integrin expression and osteopontin regulation in human fetal osteoblastic cells mediated by substratum surface characteristics, Tissue Eng. (2005), https://doi.org/10.1089/ten.2005.11.19.

[64] M. Kitsara, A. Blanquer, G. Murillo, V. Humblot, S. De Bragança Vieira, C. Nogués, E. Ibáñez, J. Esteve, L. Barrios, Permanently hydrophilic, piezoelectric PVDF nanofibrous scaffolds promoting unaided electromechanical stimulation on osteoblasts, Nanoscale (2019), https://doi.org/10.1039/c8nr10384d.

[65] D. Gupta, J. Venugopal, S. Mitra, V.R. Giri Dev, S. Ramakrishna, Nanostructured biocomposite substrates by electrospinning and electrospraying for the mineralization of osteoblasts, Biomaterials (2009), https://doi.org/10.1016/j.biomaterials.2008.12.079.

[66] K.C. Hicok, T. Thomas, F. Gori, D.J. Rickard, T.C. Spelsberg, B.L. Riggs, Development and characterization of conditionally immortalized osteoblast precursor cell lines from human bone marrow stroma, J. Bone Miner. Res. (1998), https://doi.org/10.1359/jbmr.1998.13.2.205.

[67] S.A. Harris, R.J. Enger, L.B. Riggs, T.C. Spelsberg, Development and characterization of a conditionally immortalized human fetal osteoblastic cell line, J. Bone Miner. Res. (1995), https://doi.org/10.1002/jbmr.5650100203.

[68] J.R. Jones, O. Tsigkou, E.E. Coates, M.M. Stevens, J.M. Polak, L.L. Hench, Extracellular matrix formation and mineralization on a phosphate-free porous bioactive glass scaffold using primary human osteoblast (HOB) cells, Biomaterials (2007), https://doi.org/10.1016/j.biomaterials.2006.11.022.

[69] A.R. Rafieerad, A.R. Bushroa, B. Nasiri-Tabrizi, S. Baradaran, A. Amiri, S. Saber-Samandari, S. Khanahmadi, E. Zeimaran, W.J. Basirun, K. Kalaiselvam, K. M. Vellasamy, J. Vadivelu, Simultaneous enhanced antibacterial and osteoblast cytocompatibility performance of Ti6Al7Nb implant by nano-silver/graphene oxide decorated mixed oxide nanotube composite, Surf. Coatings Technol. (2019), https://doi.org/10.1016/j.surfcoat.2018.12.119.

[70] P.J. Marie, Human endosteal osteoblastic cells: relationship with bone formation, Calcif. Tissue Int. (2015), https://doi.org/10.1007/BF03354642.
[71] T. Razafiarison, U. Silván, D. Meier, J.G. Snedeker, Surface-driven collagen self-assembly affects early osteogenic stem cell signaling, Adv. Healthc. Mater. (2016), https://doi.org/10.1002/adhm.201600128.
[72] R. Huang, L. Zhang, L. Huang, J. Zhu, Enhanced in-vitro osteoblastic functions on β-type titanium alloy using surface mechanical attrition treatment, Mater. Sci. Eng. C. (2019), https://doi.org/10.1016/j.msec.2018.12.082.
[73] H. Yang, S. Chen, L. Liu, C. Lai, X. Shi, Synthesis, characterization and osteogenesis of phosphorylated methacrylamide chitosan hydrogels, RSC Adv. (2018), https://doi.org/10.1039/c8ra05378b.